Journal of Building Engineering 122 (2026) 115790

Contents lists available at ScienceDirect

Journal of Building Engineering

journal homepage: www.elsevier.com/locate/jobe

Electrochemical behaviour of steel in low carbon cement mixtures: Insights into corrosion and passivation dynamics

M. Macht [a,*], M. Fedel [a], M.B. Valcarce [b], M. Vazquez [b], G. Speranza [c], M.C. Prestifilippo [d], D. Vaccari [d], S. Rossi [a]

[a] Department of Industrial Engineering, University of Trento, Via Sommarive 9, 38123, Trento, Italy
[b] Facultad de Ingeniería, INTEMA, Universidad Nacional de Mar del Plata, Consejo Nacional de Investigaciones Científicas y Técnicas, Colon 10850, 7600, Mar del Plata, Argentina
[c] Fondazione Bruno Kessler, Via Sommarive 18, 38123, Trento, Italy
[d] Kerakoll Green Lab, Via Pedemontana, 25, 41049, Sassuolo, MO, Italy

ARTICLE INFO

Keywords:
Corrosion
Steel
Sustainable cements
Suspension
Passivation
CSA
BOF slag

ABSTRACT

The development of alternative compositions as solutions to the environmental challenges posed by standard Portland (PTL) cement has heightened interest in their corrosion properties. Since cement is primarily used in reinforced concrete, understanding corrosion is crucial for ensuring the structural integrity of constructions. However, current studies remain insufficient to fully characterize early-age passive film behaviour. Data are still missing regarding passive-film composition in alternative cements, early-age corrosion responses, and metal exposure to pore solutions representative of real cement mixtures. This study investigates the electrochemical behaviour of carbon steel reinforcement bars in various cement environments. The analyses include a mixture of PTL cement with calcium sulfoaluminate (CSA) and CEMIII/B cement, a low-clinker cement, both compared to standard PTL cement. Electrochemical tests were conducted using two main setups: a cement extract solution and a 24-h curing environment. Electrochemical and surface-analysis techniques were combined to assess early-age corrosion behaviour and passive-film composition.

The alternative cements created different environments in terms of pH and pore solution chemistry. In the cement extract solution, the least protective passive layer was the one generated in PTLCSA, followed by the CEMIII/B and the PTL. The drop in pH in PTLCSA had a marked impact in the passive layer properties. In the curing setup, the least protective was the CEMIII/B followed by PTLCSA and PTL. In this case, the accelerated hydration properties of the PTLCSA reduced pore solution availability and corrosion activity. In conclusion, the alternative cements generate a less protective passive layer than the PTL cement and have different corrosion responses. PTLCSA could have a corrosion resistance closer to PTL for the first 24 h, but in the long run, the most similar of the alternative cements it is the CEMIII/B the one behaving similar to PTL.

* Corresponding author.
E-mail address: mateo.macht@unitn.it (M. Macht).

https://doi.org/10.1016/j.jobe.2026.115790
Received 3 October 2025; Received in revised form 12 February 2026; Accepted 3 March 2026
Available online 7 March 2026

1. Introduction

The production of cement used to produce concrete generates between 7 and 8% of the CO_2 produced globally [1]. This aspect induces great interest in reducing the amount of CO_2 produced by concrete production.

Considering that the main contributor to the CO_2 emissions is the clinker production, the substitution of the binder has been the main strategy to solve the problem. The main substitutes are primary and secondary cementitious materials. Some examples of these materials are fly ash, ground granulated blast furnace slag, limestone, silica fume, natural pozzolana, and natural calcined pozzolana [2]. According to the BS8500-2:2023 standard [3], these cement compositions can be classified into different categories according to the composition [4].

In this study, two main solutions are taken into account. The first is a mix of ordinary PTL cement with CSA that is proven to have a reduced environmental impact primarily due to the reduced amount of limestone needed in the raw feed and improved energy efficiency [5]. Furthermore, it offers the advantage of having a shorter hydration time [6]. The second is a cement CEM III/B, a low clinker cement that is produced by adding slag to the furnace and thereby producing less clinker and reducing the CO_2 footprint. This kind of cement is typified in the standard [3] as the cement mixture that produces the least amount of CO_2 per ton. The main problem with both cements is the possible low pH environment produced in the pore solution that deteriorates the passive layer [7]. CSA cements are proven to have a lower alkalinity than PTL cement [8]. In the case of the CEM III/B cement, the lower pH is due to the lower content of clinker which is composed of basic oxides. This passive layer is an iron oxide layer formed naturally in the surface of steel that prevents further corrosion [9,10]. In concrete, it is developed in the early stages when the steel comes in contact with the alkaline environment and the cement paste is still in the hydration period. The evolution of the environment and the way in which steel responds during the hydration period determine the passive layer properties. In this case, the passive layer forms, and it is stable, at a pH values higher than 12 [11]. In ordinary PTL cement, the environment around the steel bar provides the basic environment for the formation of this oxide layer. Also, given that the steel undergoes a high-temperature process during the production of the rebars, oxygen from the surrounding atmosphere reacts with the hot metal surface, leading to the formation of a stable oxide layer [12], which may be beneficial for corrosion properties. In the past, several authors worked in different cement mixtures. Achenbach et al. [13–15] performed studies on several combinations of cement mixtures, like PTL, CSA cement, CEM III/B, and also adding several components like meta-illite, metakaolin or basic oxygen furnace (BOF) slag. With these cement mixtures, aging studies of cured samples were performed, measuring open circuit potential (OCP) and performing an electrochemical impedance spectroscopy (EIS) each day. Also, at the end of a 28 days period a potentiodynamic curve is performed. In addition, the authors show chloride penetration tests and a study of the depassivation behaviour that the chlorides induce. Glawe et al. [16] study the carbonation of cement, a key factor that lowers pH and promotes corrosion, by comparing the usual method of phenolphthalein and nuclear magnetic resonance (NMR) techniques. In the present study, the main idea is to isolate the metal behaviour from the mortar by using a cement extract. Also, with a curing setup the properties of the passive layer during the hydration period were studied with the goal to understand the yielded electrochemical properties in each cement. Low-carbon cements have different hydration mechanisms that affect the passivation dynamics of steel during the process. Understanding the corrosion response of the steel to that change is crucial to understand the protection of steel in real structures.

Shi et al. [17] studied the early age passivation and long-term corrosion of carbon steel bars in PTL cement, red mud mortar, and alkali-activated slag mortar. They found that steel in mortars produced from low carbon footprint cement has a lower passivation due to their enhanced electrical resistivity. This decreases the durability of steel in the different cements, presenting signs of corrosion earlier in its service life. Given the complexity of the matrices, it becomes a difficult task to characterize the different cement compositions in corrosion terms. Unlike previous studies that analyse a certain geometry and various amounts of mixtures, this work presents a comparison between different types of geometries in the different mixtures to have an approach to the real setup.

Identifying a proper setup to study the electrochemical behaviour of steel in cementitious matrices is a key matter due to the complexity of the environment in which steel is embedded. As mentioned before, different studies were performed with a variation of different setups to overcome these difficulties. The main complexity lies in the changing environment that the concrete provides. For these reasons, several authors choose to work in a simulated pore solution [18,19]. However, this could be suppressing other effects of the mortar or concrete. Others take the approach of using a solid sample, adding complexity to the study but making it closer to reality [14]. Also, the time of the immersion during the hydration of the cement is not usually studied leaving the starting conditions as an unmeasured parameter. The setup plays an important role on surface conditions and representation of real condition, making this choice a key factor to be defined.

To evaluate how different cement compositions affect steel rebar corrosion and to evaluate the properties of the oxide layer on the surface, an initial study was conducted using a leachate setup where steel bars were immersed in cement suspension mimicking concrete pore water. This method isolates the steel from mortar effects, allowing a simpler analysis of corrosion behaviour. Cyclic potentiodynamic polarizations (CPP) were used to assess passivity and corrosion potential, while EIS provided insights into protection properties of the oxide on the surface [20]. Also, the same liquid environment was used for samples with a polished surface and 24 h of immersion to passivate the surface. Finally, a setup with solidifying concrete was used to study the evolution of the electrochemical properties during the first 24 h of hydration to investigate if the steel would passivate during that time. These studies are important to understand what is the state of the steel's passive layer before any immersion if the samples are cured in air. This affects the overall.

This study investigates the evolution of passivity during the most critical period of concrete's service life, specifically while the concrete cures and hardens. To address environmental concerns, two alternative cement types, CSA and blast-furnace slag cement (CEM III/B), were selected to reduce the CO_2 footprint associated with concrete production. The electrochemical behaviour of carbon steel in these novel cement suspensions will be compared against a baseline established after 24 h of exposure in conventional cement

suspensions.

A key emphasis of this research will be on correlating the fundamental properties of the passive oxide layer, as obtained from ex-situ X-ray photoelectron spectroscopy (XPS) analysis, with the in-situ electrochemical response observed during the curing and early hardening stages. This integrated approach aims to provide a comprehensive understanding of how the chemical composition, thickness, and integrity of the passive film directly influence the corrosion protection afforded by these alternative concrete formulations under evolving environmental conditions.

2. Methods and materials

2.1. Working electrodes preparation

To evaluate the effect of natural iron oxides, present in the commercial bars on the passivity behaviour of carbon steel, two types of electrodes were considered, one with as received bars (not polished) and the others with a polished to 1000 grit bare steel surface.

The as received steel rebars were used as working electrodes for electrochemical tests were 3 cm long, nerved bars with a nominal diameter of 12 mm and a typical composition [21] showed in Table 1. They were covered with a commercial insulating glue in the extremes to leave a 1 cm section exposed with a total nominal area of 38 mm^2. The electrical connection was established through an internal threaded socket in the working electrode and a plastic-encased screw with an exposed metal tip. A rubber ring was placed between the two components to prevent water intrusion at the connection point.

Electrodes with a bare steel surface were prepared by cutting steel rebars into disks. This procedure consisted of immersing the steel disks in a solution of concentrated nitric acid for 24 h before immersing it in resin to generate an oxide layer and avoid crevice corrosion [22]. The sample was then attached by soldering a copper wire to one of the faces of the disk and the steel sample was embedded in epoxy resin. The samples were mechanically polished using 1000 grit emery paper. The exposed sample area was 0.554 cm^2.

2.2. Electrochemical techniques

CPPs were conducted using a three-electrode setup. The reference electrode used was Hg/HgO with 0.1 mol/L KOH (149 mV vs SHE), and counter electrode was a platinum strip. The samples were immersed for 24 h to ensure a stable OCP value. The potential sweep was from 0 V vs OCP, with a vertex potential of 0.8 V vs OCP, and a final potential of 0 V vs OCP, and a scan rate of 0.1 mV/s.

EIS was performed with a conventional three-electrode setup with 50 logarithmically spaced frequencies from $2 \times 10^4 Hz$ to $5 \times 10^{-3} Hz$ with a voltage amplitude of 10 mV. The reference electrode and counter electrode used the same as in the CPPs.

For the case of the tests in the solidifying environment the reference electrode was Ag/AgCl with 3 mol/L KCl (197 mV vs SHE) which was introduced in a separate container with a 0.1 mol/L of Na_2SO_4 and connected using a salt bridge prepared with the same solution. The counter electrode is a titanium bar. Also, the frequency range was from 10 kHz to 10 mHz.

2.3. Curing mixture

To study the interaction between the steel bar and the curing cement paste a setup involving curing setup was developed. This setup had the goal to mimic the environment that the steel is embedded into while the cement is curing.

The cell for this setup, shown in Fig. 1, consisted of a ceramic container covered on the inside with filter paper to prevent the cement from sticking to the ceramic wall. The main goal of having a porous material to cover the cement was to mimic the real environment in which the cement is usually cured, allowing the exchange of gases. The working electrode, prepared as described in section 3, was submerged in the cement paste with the titanium bar as counter electrode. The fresh cement pastes were prepared with a mixing ratio of 0.135 w/s for the PTL and PTL + CSA cements and 0.12 w/s for the cement CEM III/B. This was indicated by the manufacturer for the general preparations of the cement mixtures to reach a uniform consistency. The preparation of the PTL cement mixture was prepared with 30% of Portland cement, 44% of 500-1500 μm sand and 26% 1,8-3 mm grain. The PTL + CSA was prepared with 6% anhydrite, 15% Portland cement, 9% CSA, 44% 500-1500 μm sand and 26% 1,8-3 mm grain. The CEM III/B mixture was prepared with 30% pure CEM III/B 42,5N-LH/SR, 1% chloride-free powder accelerator (Hycon A7600F, BASF SE), 43% of 500-1500 μm sand, and 26% 1,8-3 mm grain. Then, the reference electrode was immersed in an auxiliary solution of 0.1 mol/L Na_2SO_4 and connected to the cell through a salt bridge made with the same solution.

Table 1
Typical composition of C40 carbon steel [21].

Chemical composition %					
C	S	P	N	Cu	Fe
0.22	0.05	0.05	0.012	0.8	98.868

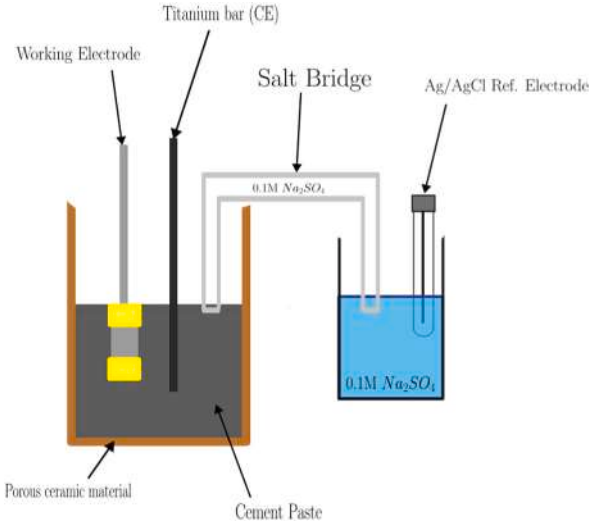

Fig. 1. Curing setup geometry.

2.4. Cement extract suspension (CES)

The cement extract solutions were prepared by mixing the cement mixture with water in a 3:1 *w/solids* relation. The suspension was not filtered, and a sediment corresponding to the insoluble parts of each cement was present. This sediment aims to act as an alkaline reserve mimicking the real environment. Every experiment was performed in the supernatant of this mixture in stagnant conditions. Also, an alternative mixture was prepared with the same *w/s* ratio with the addition of chlorides by replacing the water with a 0.1 mol/L NaCl solution. The samples that were tested in this solution were immersed for 24 h before the test to stabilize the OCP.

2.5. Thermogravimetric analysis (TGA)

A thermal analyser TGA-50 SHIMADZU (INTEMA, Mar del Plata, Argentina) was used to conduct this study, enabling the TGA and the derived thermogravimetric curve (DTG) to be obtained simultaneously on each sample. Each sample was heated from 20 to 1000 °C using a 10 °C/min heating rate.

2.6. X-ray fluorescence spectroscopy (XRF)

XRF was used to identify the elements present in the samples. Samples were analysed using a PW4025/24 Minipal2 X ray spectrometer Panalytical (INTEMA, Mar del Plata, Argentina) with Cr anode. Tests were performed without filters, under helium atmosphere at 20 kV and 5 μA with a time of 120 s.

2.7. X-ray diffraction (XRD)

XRD was used to identify components present in the samples. Samples were analysed using a IPD3000 diffractometer (Ital structures, Italy) employing a Cu Kα emission source ($\lambda = 1789$ Å). Spectra was processed using HighScore (Malvern PANalytical) with the database PDF-2 (2003).

2.8. X-ray photoelectron spectroscopy (XPS)

The chemical composition of the surface of carbon steel samples was analysed using XPS on an Axis DLD Ultra instrument (Kratos, Manchester, UK). Wide-scan spectra were recorded over a binding energy (BE) range of 1300 to −5 eV with a pass energy of 160 eV. High-resolution core-level spectra were acquired using a pass energy of 20 eV and an energy step of 0.05 eV.

When needed, charge compensation was applied. Flood gun parameters were optimized by maximizing the peak intensity and minimizing the full width at half maximum (FWHM) of the main core-line peaks. The energy scale was calibrated using the C–H bond at 285.0 eV in the C 1s spectrum as a reference. The final energy resolution was approximately 0.30 eV.

XPS spectra were processed with XPSpeaks 4.1. Shirley background subtraction and Lorentian-Gaussian components were used for fitting the core line spectra. Chemical bonds were assigned using other studies as reference [23–26].

3. Material characterization

The cementitious material was provided by Kerakoll GreenLab (Sassuolo, Mo Italy). They provided three cement mixtures identified as PTL, PTLCSA and CEM III/B. Then, to characterize even further the mixtures, several studies where performed.

3.1. Thermogravimetric analysis

A TGA of three concrete samples of different composition was performed. The preparation of the samples consisted of mixing 10 g of the three mixtures with water to reach a uniform consistency. The w/s relation for the cement was the same as used for the curing setup. Then they were cured for 24 h in a plastic container in air and crushed with mortar and pestle. The results show a clear difference between the three cements, showing three different mass changes at 80 °C, 440 °C, and 750 °C (see Fig. 2). These changes can be attributed to the calcination of Ettringite, Portlandite, and $CaCO_3$ respectively [27]. Given that each change is associated with a decomposition reaction, a mass percentage was calculated.

In Table 2 the percentage of Portlandite, calcium carbonate and Ettringite are shown. As expected, the PTL cement showed the greatest amount of Portlandite, followed by the PTLCSA and the CEM III/B. This component plays a key role in corrosion given that it acts as an alkaline reserve for the steel passivation. Regarding the calcium carbonate content, the three cements presented a similar amount. Conversely, the content of Ettringite, was the highest in the PTLCSA mixture which was expected given that the CSA promotes Ettringite formation.

3.2. X-ray fluorescence

The composition of the three cements obtained from XRF are shown in Table 3. The main differences that could be observed from this composition are the chlorine content and the sulphur content. The high sulphur content in PTLCSA mixture is explained by the CSA that was added to the cement. On the other hand, the chlorine content could correspond to chloride ions, that, in suspension, induce localized corrosion.

3.3. X-ray diffraction

XRD was performed on the cements and on the solid residues obtained by filtering and evaporating 3:1 w/s ratio suspensions of each cement. The cements were tested as provided by the company in a mix of 1:2:4 of cement, sand and gravel. The solid residues were obtained by mixing the cement mixture mentioned before in a relation 3:1 w/s, filtering the insoluble and evaporating the remaining solution at 80 °C in a clean crystallizer. The solid residues of each cement were picked up and analysed by XRD. The results in Table 4 show the mineral composition extracted from XRD analysis of the spectra in Fig. A1, A2 and A3. In all the cement types it could be observed the different calcium, aluminium and silicon oxides and the hydrated version of them in the suspension form. In the PTLCSA a greater presence of the sulphate ions was evident which correlates with the addition of the sulphate compound added. Also, different iron compounds were detected. In PTL and CEM III/B cement the iron was detected as an oxide, while in PTLCSA was detected as a sulphide. This sulphide content, given that it was also present in suspension, must be taken into consideration given that is an aggressive agent that can induce localized corrosion [28].

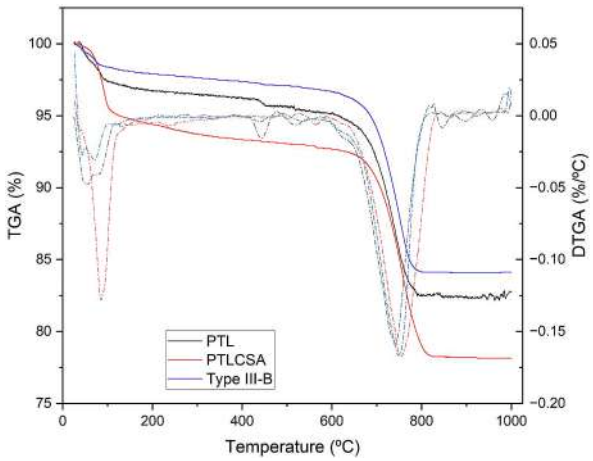

Fig. 2. TGA and DTGA for the three cements. The scan was done from 25 °C to 1000 °C in atmospheric air. Scan rate 10 °C/min.

Table 2
Mass percentage calculated from TGA using the decomposition reactions [27].

%	PTL	PTLCSA	CEM III/B
Portlandite	1.97	0.70	0.21
$CaCO_3$	28.87	32.80	28.57
Ettringite	7.99	19.75	5.00

Table 3
Oxide composition extracted from XRF analysis.

	Al_2O_3	SiO_2	SO_3	Cl	K_2O	CaO	TiO_2	Fe_2O_3
PTL (%)	7,41	3,30	1,60	0,04	1,20	78,78	0,33	7,34
PTLCSA (%)	7,80	3,20	7,10	0,02	1,10	74,39	0,47	5,93
CEM III/B (%)	8,00	4,60	1,80	0,08	1,20	78,65	0,58	5,10

Table 4
Mineral composition extracted from XRD analysis.

	Mixture	In solution
PTL	MgO	$CaCO_3$
	$CaO{\cdot}8(H_2O)$	$(Mg_{0,06}Ca_{0,94})CO_3$
	$Al_2O_3(CaO)_3{\cdot}6(H_2O)$	$Ca(SO_4){\cdot}2(H_2O)$
	$CaCO_3$	$Ca(OH)_2$
	Fe_3O_4	$Al_4(SO_4)(OH)_{10}{\cdot}7H_2O$
	SiO_2	
PTLCSA	$CaCO_3$	$CaCO_3$
	$Ca(SO_4)$	$Ca(SO_4)2(H_2O)$
	$Al_2(SO_4)_3$	$Ca(OH)_2$
	$(CaO)_{12}(Al_2O_3)_7$	$Al_2(SO_4)_3{\cdot}18H_2O$
	SiO_2	FeS
	FeS_2	
CEM III/B	$CaCO_3$	$CaCO_3$
	CaO	$2CaSiO_3{\cdot}H_2O$
	SiO_2	$Ca(OH)_2$
	Ca_2SiO_4	
	FeO	

3.4. X-ray photoelectron spectroscopy

XPS spectra was recorded on the polished carbon steel samples exposed for 48 h to the different cement suspensions. Fig. 3b, e and h show the deconvolution of peaks Fe2p3/2 for the three cements. The Fe2p3/2 peak was fitted with components of Fe(II), Fe(III) and $Fe_2(SO_4)_3$ [23–26]. The parameters obtained from the deconvolution are shown in Table 5. The contribution of Fe^0 was negligible for all cases demonstrating that the superficial layer was thicker than 10 nm. The noise in the measurements is tentatively attributed to a highly porous passive film [29]. Given that the samples were polished before immersion and that there was no contribution from Fe^0 to the signal, the porosity of the surface had to be caused by the immersion environment indicating that some components of the suspension were adsorbed in the surface. This would generate a thickening of the layer by inclusion of other components that are present in solution.

The sample immersed in PTL showed the strongest signal and a relation of Fe(III)/Fe(II) of 1.3. This value is coherent with literature values [23] of passive layer grown in saturated calcium hydroxide. In comparison the sample immersed in PTLCSA shows lower higher level of noise, that is usually correlated with a more porous layer [23], and a relation of Fe(III)/Fe(II) was 1.6 indicating less Fe(II) rendering the passive layer weaker given that Fe(II) is associated to a better corrosion resistance [29]. In the case of the sample immersed in CEM III/B the signal indicated a composition with a predominance of Fe(II) being almost the only oxidation state of iron present. As mentioned before, the Fe(II) is associated with a better corrosion resistance, but also the thickness of the passive layer affects this effect. Given that the layer was thicker than 10 nm in every case this parameter could not be compared.

Regarding the O1s signal showed in Fig. 3c, f, i, the three cement suspensions presented contributions of O^{2-}, OH^-, H_2O and C-O and C=O bonds that come from carbonates. For all samples the main contribution was OH^- that could come not only from iron hydrated oxides but from other hydroxide compounds that were present in the suspension. One of the main components contributing to that could be portlandite. The O^{2-} contribution was small in all the samples, however, the one that had the major contribution of this component is the sample that was immersed in PTL indicating a higher presence of iron oxides. The contribution of the carbonates to the signal also indicates a higher amount of carbonates in the PTL and PTLCSA, while in the CEM III/B this contribution is significantly lower. Also, the presence of sulphates was higher in the sample immersed in PTLCSA due to the higher content of sulphates in the mixture.

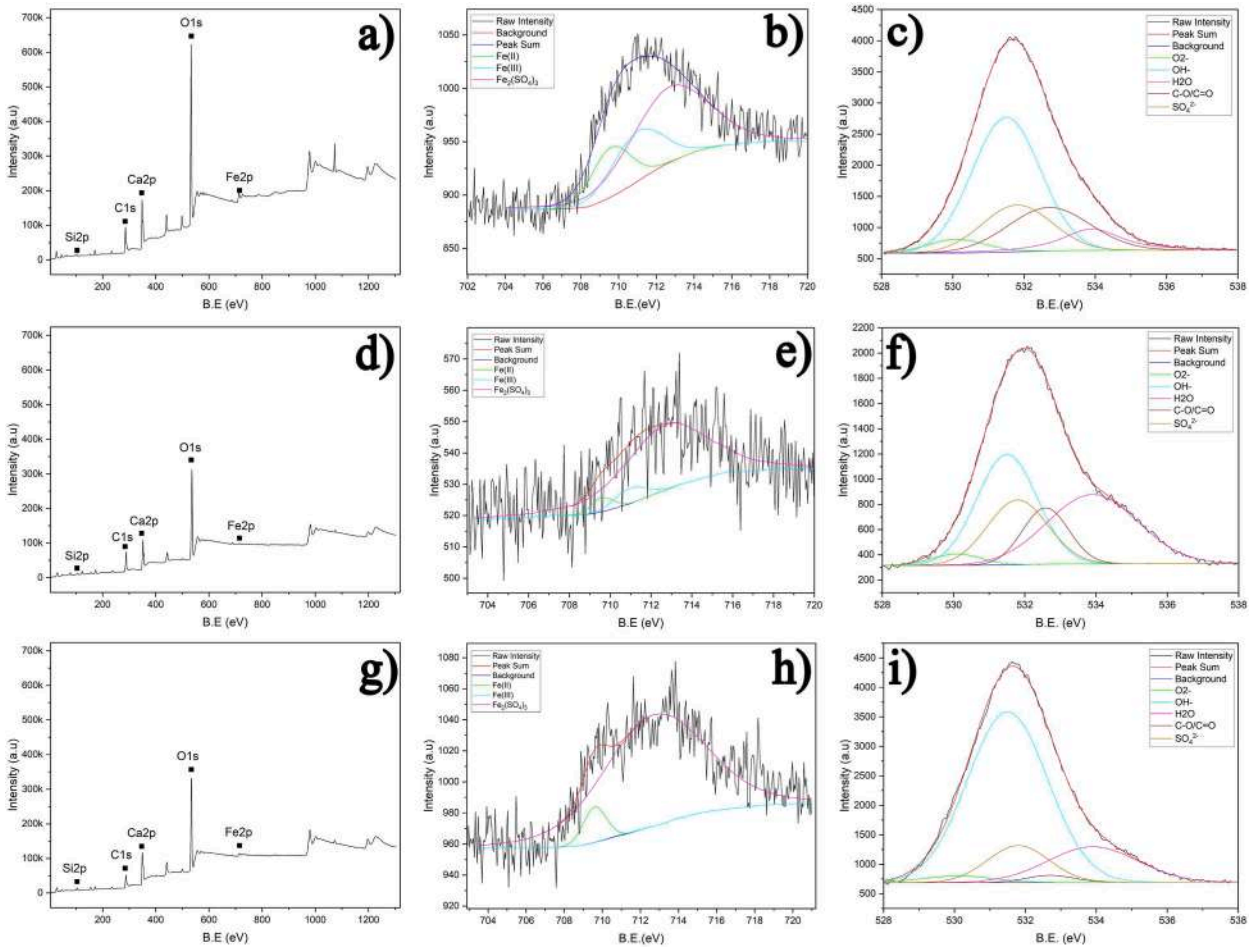

Fig. 3. XPS spectra (a,d,g), Fe2p 3/2 peak (b,e,h), and O1s (c,f,i) for steel sample immersed in PTL (a,b,c), PTLCSA (d,e,f) and Type III-B (g,h,i) cement mixtures.

Summing up, all the samples showed that the protective layer was contaminated with adsorbed species. The sample immersed in PTL demonstrated lower porosity in the superficial layer and a layer composed with oxides and carbonates. The PTLCSA demonstrated the highest relation of Fe(III)/Fe(II) rendering the passive layer weaker and a more similar percentage of carbonates than the PTL. Lastly, the CEM III/B showed a mid-range porosity and a predominance of Fe(II) in the layer with a lower presence of carbonates.

4. Electrochemical tests

4.1. Polished surface electrode immersed in cement mixtures with a passivation time of 24 h

This section presents the analysis of the results for the passivation behaviour of the mild steel samples immersed in cement mixtures with a passivation time of 24 h. The EIS data was taken after the passivation time and subsequently the CPP was measured after a stabilization time of 5 min. The sequence was performed at least three times in each CES with independent electrodes to ensure repeatability.

After 24 h of passivation the showed a stable OCP with a drift of 1 mV or less. The sample in PTL presented an OCP of -271 ± 45 mV, and the sample in PTL with the addition of chlorides showed an OCP of -270 ± 90 mV. The sample in PTLCSA presented an OCP after 24 h of -104 ± 56 mV and while the sample immersed in PTLCSA with chlorides had an OCP of -580 ± 28 mV. Lastly the sample immersed in CEM III/B presented an OCP of -302 ± 51 mV, while the sample in CEM III/B with chlorides had an OCP of -342 ± 91 mV.

Fig. 4a presents the EIS measurements after 24 h of passivation of the polished surface. The Bode plots shows the negative phase angle and the modulus of the impedance data. The data for the sample in PTL cement showed a clear passivation behaviour with a phase plateau around 80° in the middle range frequencies. The sample in CEMIII/B cement mixture showed a shorter range of the high angle plateau. The sample in the PTLCSA mixture on the other hand, showed an even smaller phase plateau, and a higher resistance of the suspension. The sample in CEMIII/B showed a weaker passivation indicated by the shorter range of the high angle plateau. This

Table 5
Parameters obtained for the fitting of the Fe2p3/2 and O1s peaks.

Condition	Peak	Compound	B.E (eV)	Area	FWHM (eV)	Composition (%)
PTL	Fe2p3/2	Fe(II)	709.6	122.397	2.48	17.64
		Fe(III)	711	159.556	3.23	23.00
		$Fe_2(SO_4)_3$	712.7	411.844	4.86	59.36
	O1s	O^{2-}	530.1	447.166	1.92	4.25
		OH^-	531.5	5212.826	2.27	49.55
		H_2O	533.9	970.558	1.94	9.23
		$(SO_4)^{2-}$	531.8	1852.619	2.32	17.61
		C-O/O-C=O	532.7	2036.173	2.70	19.36
PTLCSA	Fe2p3/2	Fe(II)	709.6	5.945	1.26	4.05
		Fe(III)	711	9.399	1.81	6.41
		$Fe_2(SO_4)_3$	712.7	131.375	4.92	89.54
	O1s	O^{2-}	530.1	155.429	1.61	2.79
		OH^-	531.5	1854.766	1.99	33.26
		H_2O	533.9	1749.701	2.99	31.38
		$(SO_4)^{2-}$	531.8	1088.825	1.99	19.53
		C-O/O-C=O	532.7	727.546	1.53	13.05
CEMIII/B	Fe2p3/2	Fe(II)	709.6	34.523	1.43	6.06
		Fe(III)	711	0.504	1.72	0.09
		$Fe_2(SO_4)_3$	712.7	534.955	6.38	93.85
	O1s	O^{2-}	530.1	277.159	2.28	2.33
		OH^-	531.5	8173.891	2.66	68.63
		H_2O	533.9	1906.396	2.98	16.01
		$(SO_4)^{2-}$	531.8	1358.407	2.04	11.40
		C-O/O-C=O	532.7	194.949	1.54	1.64

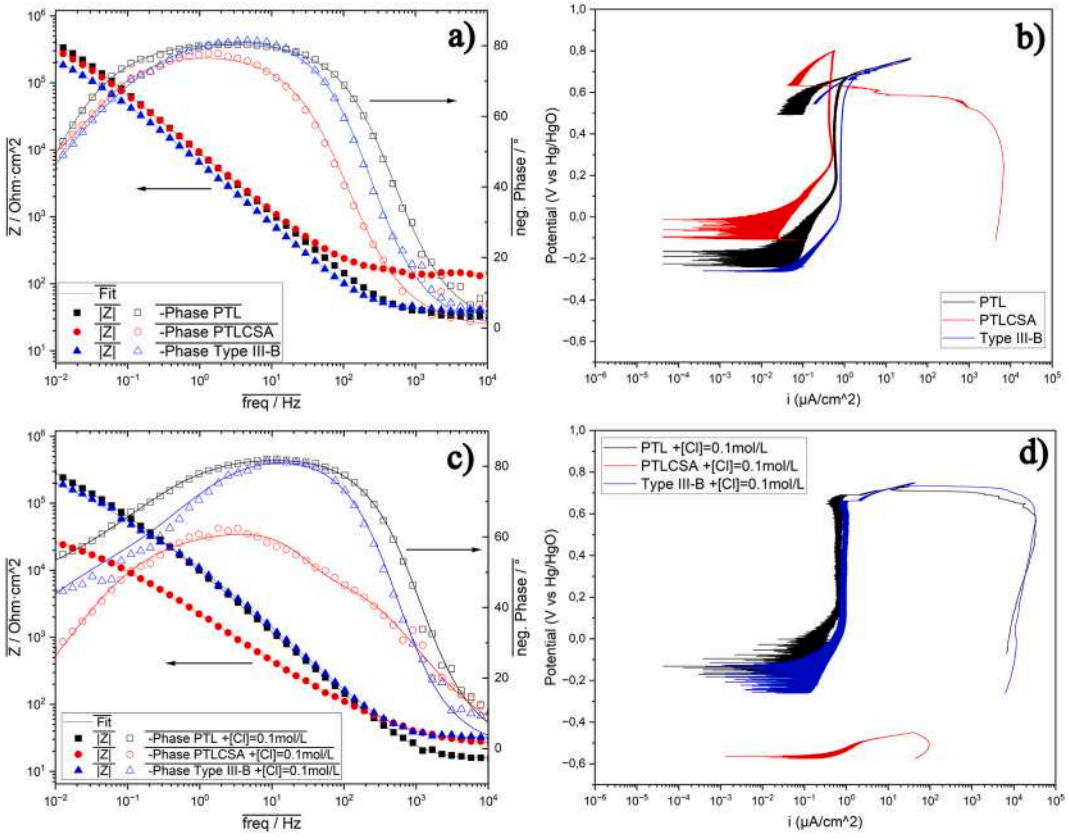

Fig. 4. EIS (a,c) and CPP (b,d) for polished sample in cement mixtures (a,b) and cement mixtures with 0.1 mol/L NaCl (c,d). In a) and c), points represent the experimental data and lines show the fitting results.

effect could be caused by the pre-existent concentration of chloride ions in the mixture that could induce defects in the protective layer, reducing the average thickness. The increased high frequency impedance modulus (representing suspension resistance) presented by the sample in PTLCSA could be correlated with the white precipitate, constituted probably by aluminium hydroxide, that appears after 24 h and decreases the amount of soluble ions, and thus the conductivity of the media. The smaller plateau in the other hand is indicative of a weaker passivation that correlates with the decreased pH to 10.8 ± 0.3 after 24 h, while the PTL and CEM III/B solutions' pH remained at 13.2 ± 0.5 and 13.1 ± 0.5 respectively.

Fig. 4b shows the CPP curves after 24 h of passivation. First, it can be seen that the corrosion potential (E_{corr}) values were lower for both, PTL and CEM III/B samples, while PTLCSA sample showed more noble potentials. Also, the passivation currents showed the same tendency, with an increasing passivation current in the order, PTLCSA, PTL, CEM III/B. However, the sample immersed in PTLCSA, after reversing the scan present pitting attack highlighted by a quickly increasing of current density, and showed hysteresis behaviour that indicates a deterioration of the passive layer. This indicates a more unstable passive layer formed by the PTLCSA mixture [30], caused by the lower pH and the presence of sulphur ions.

Fig. 4c exposes the impedance taken after 24 h of passivation of the samples in different cement mixtures with the addition of 0.1 mol/L NaCl. The impedance curve for the sample immersed in PTL mixture with chloride ions showed a lower range in the phase plateau, indicating a weaker protective layer in comparison with the setup without chlorides. The impedance modulus of this sample also showed to be the highest in comparison with the other mixtures. The sample immersed in CEM III/B mixture also followed the same tendency showing a shorter plateau than the sample immersed in PTL. The sample immersed in PTLCSA mixture however, showed a lower peak angle (60°) indicating that the behaviour is more similar to a diffusive behaviour than to a capacitor. In addition, this sample presented the lowest total impedance at low frequencies.

Fig. 4d presents the CPPs with the addition of chloride ions in the different cement mixtures. In this case, all samples in solution showed localized corrosion. After the scan is reversed no repassivation of the surface can be observed. The sample in PTLCSA with chloride ions present the worse behaviour with a low pitting potential. This tendency is explained by the pH of the solution, that decreases from 13.5 to 11 after 24 h. Given that the passivating conditions are not constant during the 24 h, the passive layer weakens and gets easily dissolved in a process that may be helped by the added chloride and the previously present sulphur ions. To assess the morphology of the corrosion processes the sample was observed under a metallographic microscope.

From this qualitative analysis, a general tendency appeared. The PTLCSA behaved as a more corrosive environment in all conditions, presenting pitting in a chloride-free environment and having significantly more active potentials with the addition of chloride ions. In the case of the CEMIII/B, the behaviour of the samples is more similar to PTL. However, CEMIII/B still showed to produce a surface layer more susceptible to corrosion than the surface layer produced in PTL. This tendency also persisted with the addition of chlorides. However, the analysis does not explain why these properties are like this and only characterize the behaviour of the samples.

The EIS data was fitted with the circuit showed in Fig. 5Fig. 5 with two time constants. The circuit was chosen given the presence of a passive layer where the capacitances were replaced by constant phase elements (CPE) to account for non-ideal behaviour. The parameters represent the resistance of the solution (Rs), the resistance of the protective layer (Rc), the charge transfer resistance (Rct), the capacitance of the protective layer (Qc) and the capacitance of the double layer film (Qdl).

The results of the fitting are exposed in Table 6 with the corresponding units. The results correspond to the curve in Fig. 4a and c and are representative of several repetitions aiming to compare the different electrochemical responses. In almost every condition, n_c values close to 1 suggest an almost ideal behaviour of the capacitive response associated to the presence of a protective passive layer in the high-frequency region [31–33]. This film shows Rc and Rct values that increase, with lower Qc values as expected for a film with better corrosion resistance. Charge transfer resistance values higher than 100 kΩ cm^2 are associated with the passive state, while values lower than 10 kΩ cm^2 are typical of actively corroding steel [34,35]. The Qc obtained for PTLCSA + Cl is higher than the rest and the n_c obtained lower than the rest. This indicates that the surface layer formed in PTLCSA + Cl had water penetration, decreasing the overall capacitance due to the higher permittivity of water. Also, this sample presents Rct lower than 50 kΩ cm^2, close to the passive-active limit.

Fig. 6b shows the surface of the electrode immersed in PTLCSA after the CPP. The surface showed pits dispersed on the electrode. Given the low depth of the pits and the amount of them, the corrosion process seemed to be dominated by the nucleation of new pits rather than by their growth This could be indicating that the pH makes the formation of new pits from sulphide ions more effective than the deepening of already formed pits. The other samples in different cement solutions without chloride ions indicate no significant corrosion while the addition of chloride ions induces a more generalized corrosion.

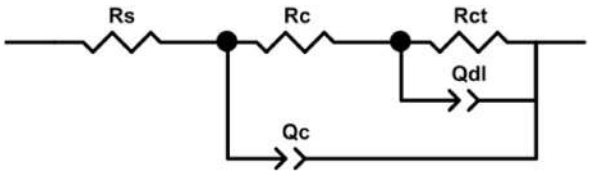

Fig. 5. Circuit used to fit the explerimental EIS data.

Table 6
Fitted parameters for EIS data of polished samples immersed in CESs.

	PTL	CEMIII/B	PTLCSA	PTL + Cl	CEMIII/B + Cl	PTLCSA + Cl
$Rs/\Omega cm^2$	32.1	40.0	140.8	15.4	32.2	23.4
$Qc/\mu\Omega^{-1}cm^{-2}S^N$	21.1	28.1	22.2	17.1	14.5	120.1
n_c	0.90	0.92	0.87	0.93	0.94	0.67
$Rc/k\Omega cm^2$	33.0	79.0	42.0	43.4	27.7	0.77
$Q_{dl}/\mu\Omega^{-1}cm^{-2}S^n$	4.5	1.23	43.7	10.6	1.69	5.66
n_{dl}	0.33	0.49	0.84	0.56	0.54	0.99
$R_{ct}/k\Omega cm^2$	1027	67.4	57.2	1541	89.0	39.9
χ^2	0.002	0.002	0.005	0.002	0.007	0.002

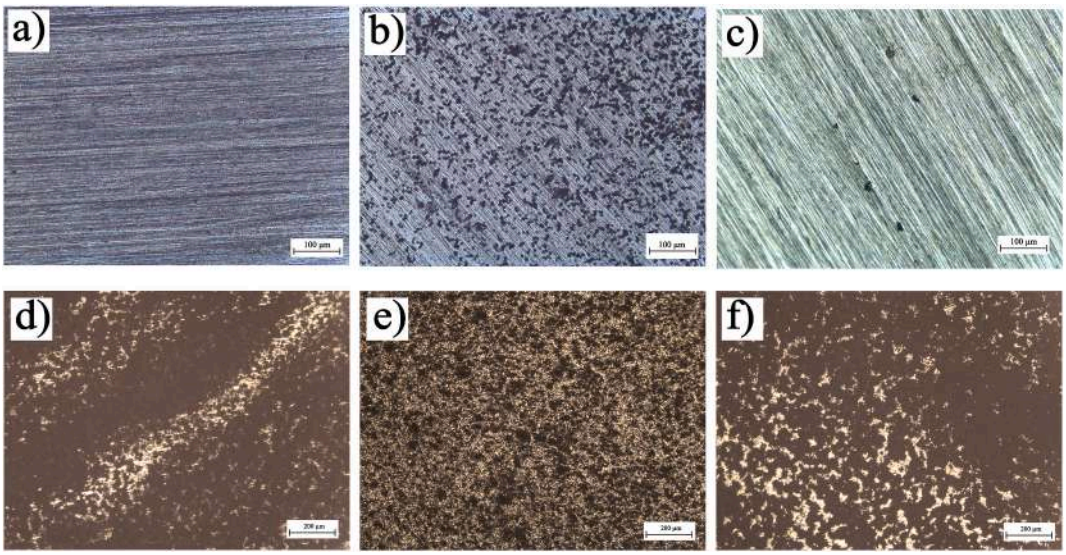

Fig. 6. Micrographs of electrodes immersed in PTL (a,d), PTLCSA (b,e) and CEMIII/B (c,f) after having carried out anodic polarization curves without chlorides (a,b,c) and with a concentration of 0.1 mol/L NaCl (d,e,f).

4.2. Rebar electrode immersed in cement mixtures with a passivation time of 24 h

In this section the same experiments were carried with a rebar electrode. The electrodes were passivated in the test suspension during 24 h. After that period, the EIS data was taken and subsequently the CPP was measured after a stabilization period of 5 min.

After 24 h of passivation the showed a stable OCP with a drift of 1 mV or less. The sample that was immersed in PTL showed an OCP of -199 ± 28 mV, and the sample in PTL with chlorides showed an OCP of -253 ± 20 mV. The sample immersed in PTLCSA showed an OCP of -403 ± 69 mV and the sample in PTLCSA with chlorides an OCP of -439 ± 30 mV. The sample immersed in CEM III/B showed an OCP of -243 ± 24 mV and the sample in CEM III/B with chlorides a value of -284 ± 60 mV.

Fig. 7a shows the impedance data after 24 h of passivation of the rebar samples. In comparison with the other electrode, it is possible to observe a decreased plateau in the phase angle for all the mixtures, indicating lower protection when the pre-existent oxide layer is present. However, a similar tendency with respect of the different cement mixtures appeared. The sample in PTL showed the greatest peak of phase angle and a higher low frequency impedance with respect to the others, demonstrating a more protective behaviour from the oxide layer to the metal with respect with the others cement mixtures. The sample in PTLCSA, shows the characteristic increased high frequency resistance corresponding to the solution properties explained before. Also, the phase angle never surpasses the 40° angle, which indicates a behaviour with a diffusive character in the low frequency range. It also presents a reduced low frequency impedance indicating higher corrosion rates. The sample in CEM III/B showed a decreased peak phase angle lower than the PTL as well as the low frequency impedance.

Fig. 7b shows the CPP for the rebar electrodes in the different cement mixtures. Comparing with the polished electrodes, the rebars

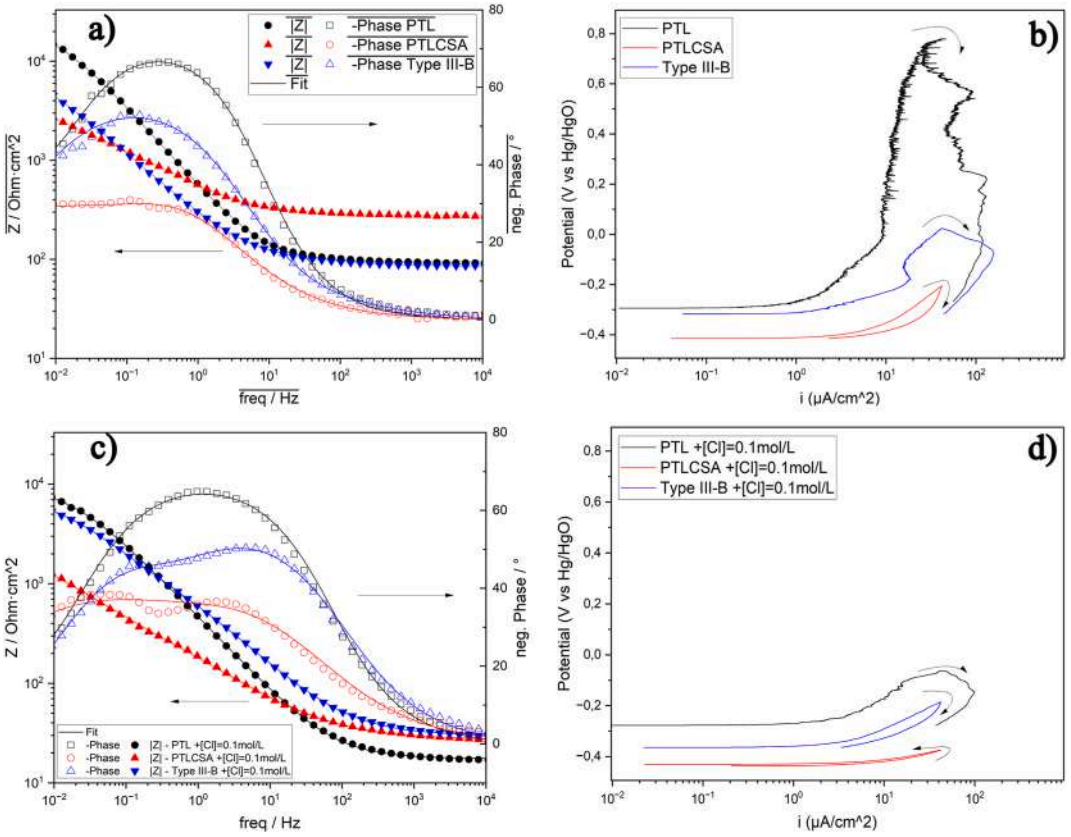

Fig. 7. EIS (a,c) and CPP (b,d) for rebar electrode in cement mixtures (a,b) and cement mixtures with 0.1 mol/L NaCl (c,d). Points represent the experimental data and lines show the fitting results.

showed an increased current in the curves and more instability. This could be attributed to the natural variance in the surface conditions. The sample immersed in PTL showed an unstable passive layer with signs of metastable pitting, a high pitting potential and no repassivation. The sample in PTLCSA shows a significantly lower E_{corr} and no signal of passivation in the current range studied. The sample in CEM III/B has a similar E_{corr} to the one in PTL and presents a week passivation showed by the decrease in current in the first branch around −178 mV vs Hg/HgO. However, the current increases again showing a weaker passivation layer than in the case of the sample in PTL.

After the CPP the samples were observed at the optical microscope. Fig. 8 shows some of the corrosion defects produced by the CPP test in each sample. The sample that was tested in PTL showed corrosion phenomenon mainly localized and small. The sample immersed in PTLCSA showed a more generalized deterioration with the presence of a white sediment in the surface concentrating in the sides of the nerves of the bar. The sample immersed in CEM III/B showed more corrosion sites with more accumulation of corrosion products than the PTL.

The experiments were repeated with the addition of chloride preparing the mixtures with a solution of 0.1 mol/L NaCl concentration. The samples were left in solution to passivate during 24 h before the EIS was executed and a later CPP after 5 min of OCP stabilization.

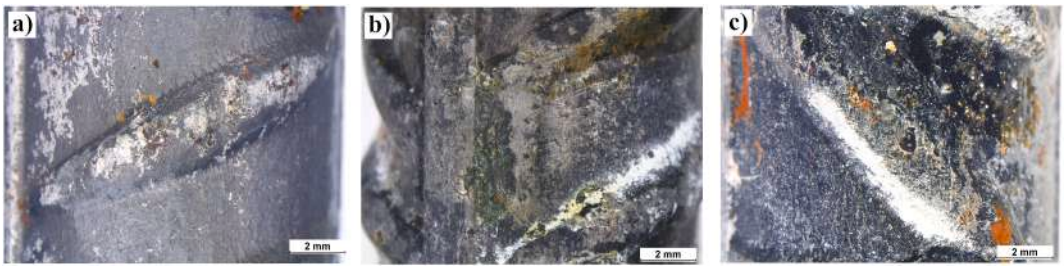

Fig. 8. Images of rebar samples after the CPP in different cement mixtures. PTL (a), PTLCSA (b), Type III-B (c).

Fig. 7c shows the EIS data for the samples in the different cement mixtures with chlorides. The sample immersed in PTL showed a peak phase angle of 65° indicating similarities with the passivation with no chlorides (Fig. 7a). This sample also showed the greatest low frequency impedance. The overall impedance showed a decreased value in comparison with the test without chlorides produced by the increased conductivity (effect at high frequencies) and aggressiveness (effect at low frequencies) that the NaCl generates. The sample in PTLCSA showed the lowest maximum phase angle around 38°, indicating a that there is no capacitive behaviour present. In addition to that, the data showed two-time constants with two different peaks, characteristic of an oxide layer that presents defects. The total impedance at low frequencies of this sample was the lowest of all. The sample immersed in CEM III/B showed a maximum peak phase at 50° showing comparatively an intermediate behaviour compared with the other mixtures. The presence of the decrease in the angle in the low frequency region and the lower impedance modulus at low frequencies also suggests a defective oxide layer.

Fig. 7d shows the polarization data for the samples in the different cement mixtures with chlorides. The sample immersed in PTL showed a E_{corr} of -276 ± 15 mV vs Hg/HgO and a maximum potential, reached at the current limit, of -62 ± 25 mV vs Hg/HgO. The test showed higher currents than in other tests and an increased in the current at a lower potential. The sample immersed in PTLCSA showed an E_{corr} of -445 ± 26 mV vs Hg/HgO and a maximum potential of -378 ± 29 mV vs Hg/HgO. The sample immersed in CEM III/B showed an E_{corr} of -328 ± 54 mV vs Hg/HgO and a maximum potential of -158 ± 72 mV vs Hg/HgO standing again in between the other two cement mixtures.

After the CPP the samples were observed at the optical microscope. Fig. 9 shows some of the corrosion defects that were found in the samples immersed in different mixtures. The sample immersed in PTL showed localized corrosion with a local increase in pH generating vertical defects due to gravity. The one in PTLCSA showed a white precipitate in the surface and corrosion that was initiated near de nerves of the bar and then expanded to the rest of the surface. The sample in CEM III/B showed a brown deposit that accumulated in the nerves of the bar. Corrosion pits were found to be nucleated in the surface without any correlation with the rebar morphology.

EIS data was fitted using again the circuit in Fig. 5 given that the mechanism was assumed to be the same. This allows the comparison between the two different surface conditions.

The fitted parameters in Table 7 are for the repetition showed in Fig. 7a and c. Three or more repetitions were made and repeatability was assured. The fitting values are representative and are exposed with the goal of comparing the electrochemical response of each sample. The experimental data with a n_{dl} of 0.5 are found to reasonably fit the proposed equivalent circuit when n_{dl} is fixed during the fitting procedure. In this case the CPE can be associated to the diffusion of Fe(II) ions through the less porous protective layer, which is the determining step in the corrosion process [36].

The results of the fitting for the rebar samples are shown in Table 7. Comparing the results with the polished samples, the effect of the pre-existent porous oxide layer affects the behaviour of the steel surface. The higher Qc and lower n_c values are explained by the penetration of water in the oxide layer that decreases the overall capacitance. Also, Rc and Rct values are lower and n_t tend to 0,5 in CEM III/B and PTLCSA when chloride ions are present. This could be attributed to the diffusion through a thicker oxide layer. It is clear, that the best condition is again PTL, given the lower values of Qc, higher n_o and higher Rct values.

In conclusion the tests showed that the CEMIII/B produced a surface layer with similar properties to the one produced in PTL, although, the corrosion resistance of the first surface layer is significantly lower than the one in PTL. The PTLCSA showed to form the least protective layer, presenting pitting even in chloride-free electrolytes. The addition of chloride ions, stressed this tendency, introducing pitting in all samples and rendering active the sample in PTLCSA after 24 h. The rebar samples showed also to have the same tendency, and the pre-existent oxide layer absorbs water and provides less protection.

4.3. Curing mixture

The results of the EIS study and potential measurement performed during 24 h for the solidifying setup are discussed in this section. The main goal of these experiments was to assess the electrochemical behaviour in the first 24 h of curing. Within this time the cement paste solidifies into a solid matrix, and this influences the aggressiveness of the environment for the steel bar affecting mass transport and porosity.

In Fig. 10a, the potential evolution of the sample immersed in PTL over the first 24 h of curing is exposed. The shape of the curve showed a first period of low potential, followed by a later increase. The initial low potential period indicates a higher activity in the first steps of the curing stage. This phenomenon could be associated to the formation of a passive oxide layer in the surface. The low

Fig. 9. Images of rebar samples after the CPP in different cement mixtures with 0.1 mol/L NaCl. PTL + Cl (a), PTLCSA + Cl (b), Type III-B + Cl (c).

Table 7
Fitted parameters for EIS data of rebar samples immersed in CESs.

	PTL	CEMIII/B	PTLCSA	PTL + Cl	CEMIII/B + Cl	PTLCSA + Cl
Rs/Ωcm^2	94.3	84.8	225.9	17.5	29.7	27.0
Qc/μΩ^{-1}cm^{-2}S^N	410	915	810	527	404	1730
n_c	0.81	0.63	0.62	0.76	0.67	0.56
Rc/kΩcm^2	24.4	0.04	1.5	9.5	1.3	0.02
Q_{dl}/μΩ^{-1}cm^{-2}S^n	2058	246	1600	8900	293	1700
n_{dl}	0.88	0.78	0.5	0.70	0.50	0.5
R_{ct}/kΩcm^2	30.0	13.1	9.6	10.0	8.5	4.1
χ^2	0.003	0.001	0.001	0.002	0.002	0.003

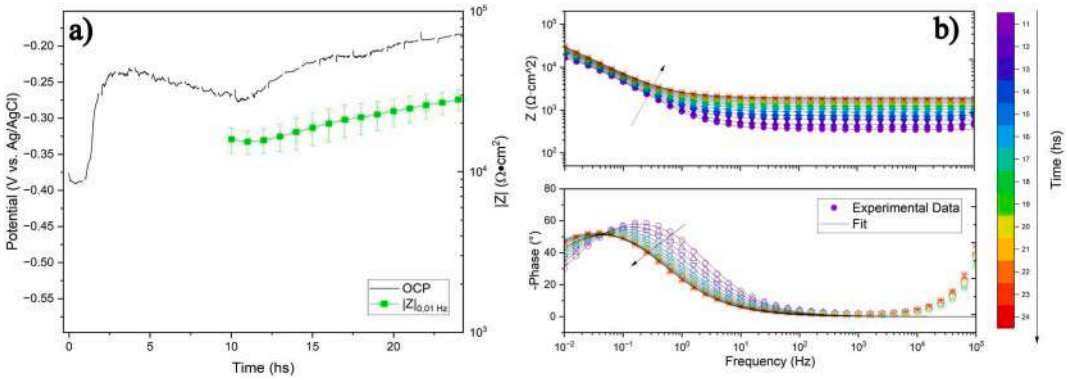

Fig. 10. OCP and impedance modulus at 0.01 Hz (a) and EIS (b) evolution during the 24 h of curing in PTL cement paste.

frequency data is also exposed in Fig. 10a for the more stable part of the OCP measurement given that it follows the corrosion process and a similar trend with the OCP was observed too.

The test performed with PTL cement showed in Fig. 10b presented an evolution of the EIS curve that demonstrated a first increase of high frequency resistance that was caused by the drying process of the cement. The phase showed a decrease in the maximum phase over time that correlates with the corrosion potential evolution. A shift in the time constant peak is also observed caused by an increase in charge transfer resistance. This could be caused by the formation of the oxide layer on the surface. The decrease of the water content would decrease the corrosion current given that the water participates in the cathodic reaction and acts as a solvent for ionic species.

The results for the sample in PTL + CSA cement showed in Fig. 11a presented fast potential ennobling, increasing OCP instantly in

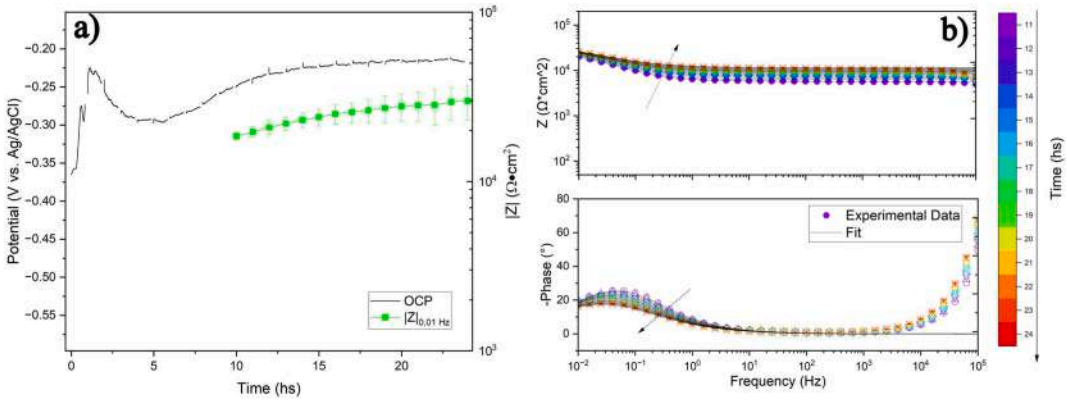

Fig. 11. OCP (black) and impedance modulus at 0.01 Hz (green) evolution during the 24 hs of curing in PTLCSA cement paste.

contrast with the other cements that have a low OCP period. This could be associated with the fast-curing properties of the cement that set the steel surface environment faster. Also, the later valley also appeared in this cement mixture at shorter times. These behaviours were very similar to the PTL cement but with a higher rate at which the properties developed. Also, the low frequency impedance data is shown demonstrating a similar tendency with the OCP.

The results exposed in Fig. 11b, show the EIS data for the 24 h of the sample immersed in curing cement paste made with PTLCSA mixture. The high frequency range indicates the variation in solution resistance. Solution resistance increased rapidly due to the solidifying of the cement, however in this case, the increment was greater and faster in comparison with other cements corresponding again to the fast-curing properties of the mixture. Also, a low peak angle phase is shown during the testing period of around 20°, meaning a more resistive behaviour. This indicates a weak contribution of the double layer. This could be caused by the different process of curing that renders the cement-metal interface in the surface with less ions to form the double layer.

The potential evolution exposed in Fig. 12a corresponds to the evolution of the sample immersed in the CEM III/B curing cement paste. The evolution showed a first activity valley, that could be indicating a slower passivation process. Also, this sample had a lower final potential, indicating that even after solidifying the metal was more active in comparison with samples immersed in other mixtures. In contrast with the other cements, the low frequency impedance did not follow the trend of the OCP in this case. The OCP around −330 mV vs Ag/AgCl and the low impedance value under 10^4 indicates a slower passivation process.

The EIS data shown in Fig. 12b demonstrated a one time constant with a decrease in peak phase and an increase in high frequency impedance corresponding to the cement resistance. The increase in the cement resistance was caused by the formation of hydration products, consumption of free water that served as conductive medium and immobilization of ions onto the surface of the hydration products. However, the decrease in peak phase is associated with a loss of the metal's capacitive character. This could be caused by the decrease of the concentration of ions in the surface by incorporation into the solid matrix.

$$C_{dl} = (Q_{dl})^{\frac{1}{n_{dl}}} \cdot (R_{ct})^{\frac{1-n_{dl}}{n_{dl}}} \quad (1)$$

The impedance results were fitted using ZSimpWin, excluding high frequency data to focus the fitting in the metal surface process. The fitted data excluded frequencies higher than 1 kHz and it was performed with a one time-constant circuit with a constant phase element instead of a normal capacitor to account for non-ideal behaviour. The Ru component represents the resistance of the curing paste, the Rct represents the charge transfer resistance to account for the electrochemical process in the metal surface and the Qdl component represents the double layer with a constant phase element due to the behaviour of a non-ideal capacitor. The equivalent double-layer capacitance was calculated using Qdl and Rct in equation (1).

The evolution of the mortar resistance (Ru) parameter is reported in Fig. 13a. The difference in mortar resistance was notable for the three cements, yielding the maximum value the PTLCSA cement, and the lowest value the CEM III/B cement with the PTL being the middle value. Also, the shape of the curve indicated a faster process for PTLCSA cement and a slower process for the CEM III/B cement in comparison with the PTL.

The charge transfer resistance (Rct) parameter is related with the corrosion process in the surface by being inversely proportional to the corrosion current. Fig. 13b shows the evolution in time of Rct for the samples in different cement pastes during time. The PTL cement showed the most favourable behaviour with an increasing Rct with time, finishing the testing period with the value over 100 kΩ cm^2 indicating a passive behaviour [37]. The sample in PTLCSA showed a more constant value over time, which is caused by the consolidated properties of the matrix at lower times. The sample in CEM III/B cement paste, on the other hand, showed a decreasing Rct indicating an increase in the corrosion rate finishing the testing period with a value under 10 kΩ cm^2 indicating an active state [37].

In Fig. 13c the values for the double layer capacitance (C_{dl}) are shown. The values were in the range of the mF due to the oxide layer pre-existing on the surface generated in manufacturing process [38,39]. A general tendency tends to appear as a decreasing capacitance with time that could be attributed to the curing of the cement and the decrease of ion concentration and water content in the matrix by incorporation into the matrix.

5. Conclusions

From these experiments, several conclusions can be drawn:

5.1. Surface chemistry

- XPS showed that different cement mixtures produce surface layers containing different amounts of Fe(II) and Fe(III).
- The electrochemical evaluation exposed that the sample in PTL showed to have the most protective ion relation. The sample in PTLCSA showed a thinner oxide layer rendering the metal more susceptible. The sample in CEM III/B demonstrated a similar percentage of Fe(II) in the formed surface layer associated with oxides and hydroxides than the sample in PTLCSA, while the Fe(III) is mainly found as $Fe_2(SO_4)_3$.

5.2. Passivation behaviour

- The passive layer behaviour deduced from the CPP curves in cement extract suspension indicated that the passive layer of steel in PTL was more protective than the alternatives.

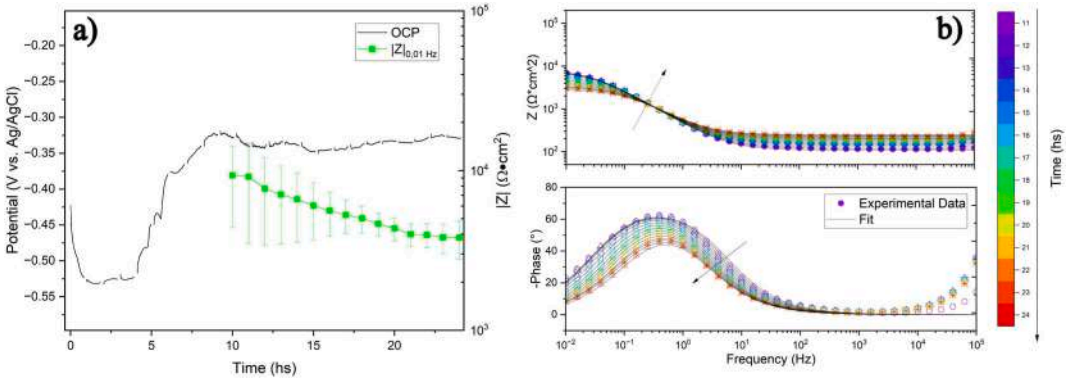

Fig. 12. OCP and impedance modulus at 0.01 Hz (a) and EIS (b) evolution during the 24 h of curing in Type III-B cement paste.

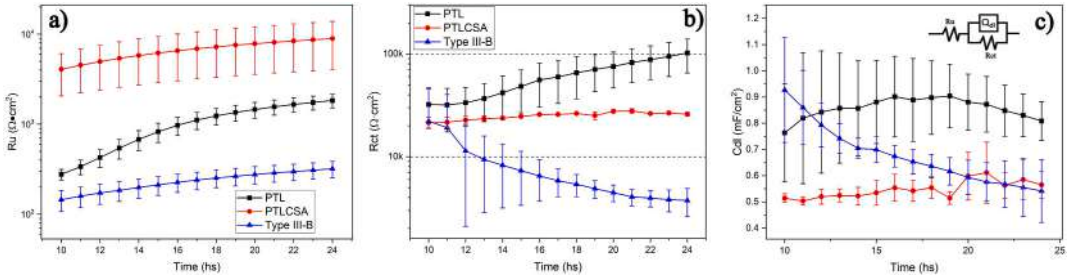

Fig. 13. Parameters fitted for the one time constant circuit for the different cement pastes. Ru(a), Rct(b), Cdl(c).

- The PTLCSA indicated the possible presence of sulphide ions that also contributes to a lower corrosion resistance. Furthermore, after 24 h the suspension has a low pH that contributes the passive layer dissolution.

5.3. Chloride ion impact

- With the addition of chloride ions, similarities in the pitting potentials of steel in PTL and CEM III/B were observed. The passivation in PTLCSA does not offer protection to the metal due to the decreased pH of the solution.
- The CEM III/B cement has a concentration of chloride ions that does not promote localized corrosion, given that the pH is high and the $[Cl^-]/[OH^-]$ is lower than 0.6.

5.4. Experimental factors

- The different setups showed that the fast hydration process of the PTLCSA favours the development of a less aggressive environment. Further studies are needed to investigate if the cement can develop a more corrosive environment after curing in different conditions.
- The different geometries of electrodes in solution demonstrated to be comparable. The rebar as received showed a more active surface caused by defects and the complex geometry.
- The curing cement setup showed similarities between the steel sample in PTL cement and the one in PTL + CSA. This study shows a behaviour dictated by the cement conditions and indicates that the CEM III/B is more susceptible to corrosion in the short term.

CRediT authorship contribution statement

M. Macht: Writing – original draft, Visualization, Methodology, Investigation, Formal analysis. **M. Fedel:** Writing – review & editing, Supervision, Resources, Funding acquisition. **M.B. Valcarce:** Writing – review & editing, Validation, Methodology. **M. Vazquez:** Writing – review & editing, Validation, Methodology. **G. Speranza:** Investigation, Formal analysis. **M.C. Prestifilippo:** Resources. **D. Vaccari:** Resources. **S. Rossi:** Writing – review & editing, Supervision, Resources, Funding acquisition.

Funding sources

Mateo Macht, Michele Fedel and Stefano Rossi gratefully acknowledge MUR for the financial support in the frame of PNRR ex DM 118/2023 Missione 4, componente 1 “Potenziamento dell'offerta dei servizi di istruzione: dagli asili nido all’Università” –

Investimento 3.4 “Didattica e competenze universitarie avanzate” e Investimento 4.1 “Estensione del numero di dottorati di ricerca e dottorati innovativi per la pubblica amministrazione e il patrimonio culturale”

Declaration of competing interest

The authors declare the following financial interests/personal relationships which may be considered as potential competing interests: Steafano Rossi reports equipment, drugs, or supplies was provided by Kerakoll SpA. If there are other authors, they declare that they have no known competing financial interests or personal relationships that could have appeared to influence the work reported in this paper.

Appendix A

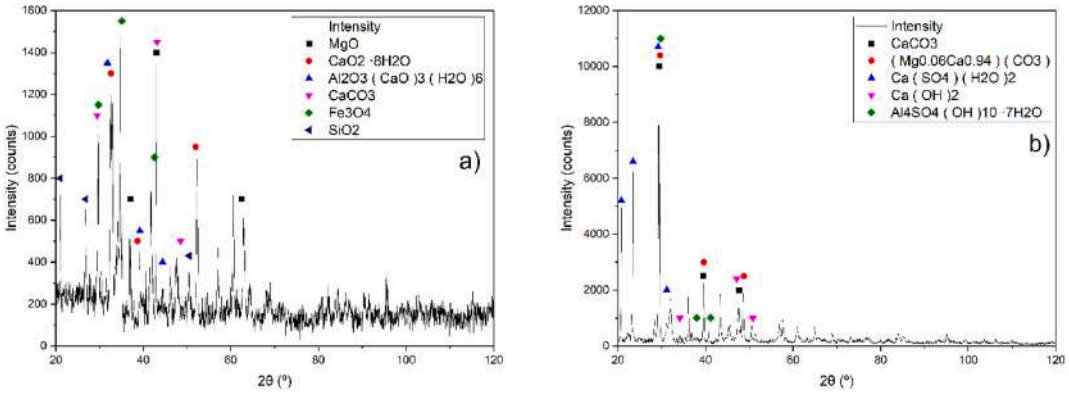

Fig. A14. XRD pattern for cement extract solution PTL(a), PTL leachate(b).

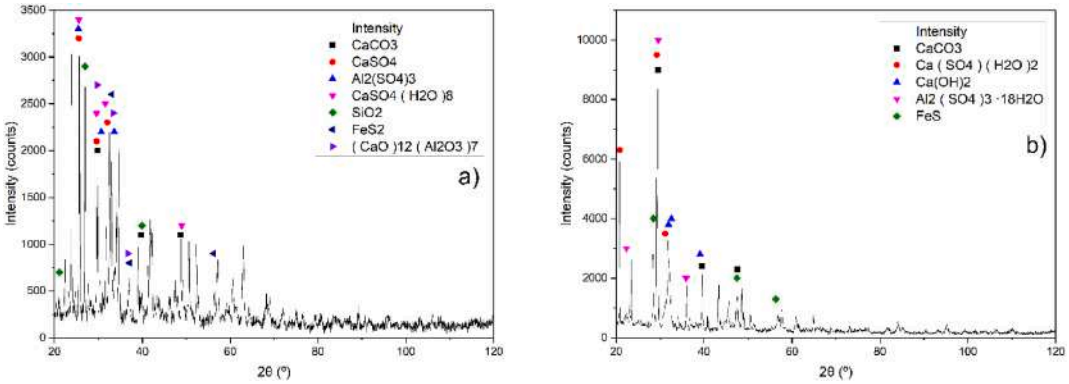

Fig. A15. XRD pattern for cement extract solution CEMIII/B(a), CEMIII/B leachate(b).

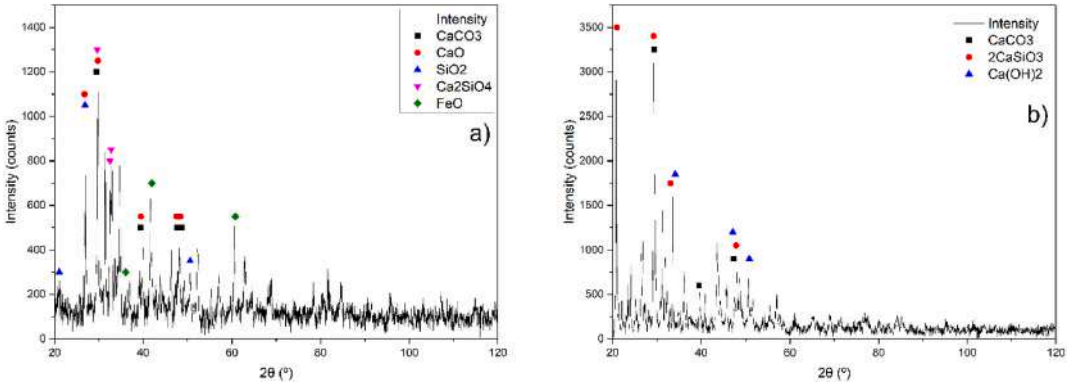

Fig. A16. XRD pattern for cement extract solution PTLCSA(a), PTLCSA leachate(b).

Data availability

Data will be made available on request.

References

[1] Y.O. Abiodun, O.A. Olanrewaju, O.P. Gbenebor, E.F. Ochulor, D.V. Obasa, S.O. Adeosun, Cutting cement industry CO2 emissions through metakaolin use in construction, Atmosphere 13 (2022) 1494, https://doi.org/10.3390/atmos13091494.

[2] S. Mundra, G. Samson, G. Masi, R. Achenbach, D.M. Bastidas, S.A. Bernal, et al., Application of electrochemical methods for studying steel corrosion in alkali-activated materials, Mater. Corros. 74 (2023) 988–1008, https://doi.org/10.1002/maco.202313743.

[3] Concrete – complementary British standard to BS EN 206 – part 2: specification for constituent materials and concrete n.d. https://doi.org/10.3403/30471317.

[4] I.H. Shah, S.A. Miller, D. Jiang, R.J. Myers, Cement substitution with secondary materials can reduce annual global CO2 emissions by up to 1.3 gigatons, Nat. Commun. 13 (2022) 5758, https://doi.org/10.1038/s41467-022-33289-7.

[5] T. Hanein, J.-L. Galvez-Martos, M.N. Bannerman, Carbon footprint of calcium sulfoaluminate clinker production, J. Clean. Prod. 172 (2018) 2278–2287, https://doi.org/10.1016/j.jclepro.2017.11.183.

[6] L.E. Burris, K.E. Kurtis, Influence of set retarding admixtures on calcium sulfoaluminate cement hydration and property development, Cement Concr. Res. 104 (2018) 105–113, https://doi.org/10.1016/j.cemconres.2017.11.005.

[7] W.K. Green, Steel reinforcement corrosion in concrete – an overview of some fundamentals, Corrosion Eng. Sci. Technol. 55 (2020) 289–302, https://doi.org/10.1080/1478422X.2020.1746039.

[8] L. Wang, S. Zhan, X. Tang, Q. Xu, K. Qian, Pore solution chemistry of calcium sulfoaluminate cement and its effects on steel passivation, Appl. Sci. 9 (2019) 1092, https://doi.org/10.3390/app9061092.

[9] M. Sánchez-Moreno, H. Takenouti, J.J. García-Jareño, F. Vicente, C. Alonso, A theoretical approach of impedance spectroscopy during the passivation of steel in alkaline media, Electrochim. Acta 54 (2009) 7222–7226, https://doi.org/10.1016/j.electacta.2009.07.013.

[10] M. Sánchez, J. Gregori, C. Alonso, J.J. García-Jareño, H. Takenouti, F. Vicente, Electrochemical impedance spectroscopy for studying passive layers on steel rebars immersed in alkaline solutions simulating concrete pores, Electrochim. Acta 52 (2007) 7634–7641, https://doi.org/10.1016/j.electacta.2007.02.012.

[11] G.Y. Koga, B. Albert, V. Roche, R.P. Nogueira, A comparative study of mild steel passivation embedded in belite-ye'elimite-ferrite and Porland cement mortars, Electrochim. Acta 261 (2018) 66–77, https://doi.org/10.1016/j.electacta.2017.12.128.

[12] O.A. Zambrano, J.J. Coronado, S.A. Rodríguez, Mechanical properties and phases determination of low carbon steel oxide scales formed at 1200°C in air, Surf. Coat. Technol. 282 (2015) 155–162, https://doi.org/10.1016/j.surfcoat.2015.10.028.

[13] R. Achenbach, M. Raupach, Comparative investigation on the influence of metakaolin, metaillite and steel slag as SCMs in mortar on the corrosion behavior of embedded steel, Koroze Ochr Mater 67 (2023) 21–32, https://doi.org/10.2478/kom-2023-0004.

[14] R. Achenbach, M. Raupach, Passivation of steel reinforcement in low carbon concrete, Buildings 14 (2024) 895, https://doi.org/10.3390/buildings14040895.

[15] Achenbach R, Raupach M. Suitability of rapid chloride migration tests for determining the migration coefficient in mortars made from different novel binder types. Mater. Corros. n.d.;n/a. https://doi.org/10.1002/maco.202414369.

[16] C. Glawe, F. Georget, M. Raupach, T. Matschei, Multi technique characterization of the carbonation affected zone including non-destructive single sided 1H NMR, Cement Concr. Res. 178 (2024) 107438, https://doi.org/10.1016/j.cemconres.2024.107438.

[17] J. Shi, Z. Geng, X. Zhou, Reinforcing steels in low-carbon mortars subjected to chloride attack and natural carbonation: contradictory trends in passivation ability and corrosion resistance, Cem. Concr. Compos. 152 (2024) 105666, https://doi.org/10.1016/j.cemconcomp.2024.105666.

[18] F. Fei, J. Hu, J. Wei, Q. Yu, Z. Chen, Corrosion performance of steel reinforcement in simulated concrete pore solutions in the presence of imidazoline quaternary ammonium salt corrosion inhibitor, Constr. Build. Mater. 70 (2014) 43–53, https://doi.org/10.1016/j.conbuildmat.2014.07.082.

[19] M. Moreno, W. Morris, M.G. Alvarez, G.S. Duffó, Corrosion of reinforcing steel in simulated concrete pore solutions: effect of carbonation and chloride content, Corros. Sci. 46 (2004) 2681–2699, https://doi.org/10.1016/j.corsci.2004.03.013.

[20] S. Shao, M. Guo, Y. Zhang, Natural passivation and chloride corrosion resistance of Inconel 625 in OPC and CSA concrete pore solutions with different pH, Cem. Concr. Compos. 154 (2024) 105794, https://doi.org/10.1016/j.cemconcomp.2024.105794.

[21] Barre di Acciaio per Cemento Armato - pittini. Pittini.com, n.d. https://www.pittini.com/prodotti/edilizia/barre/. (Accessed 23 September 2025).

[22] M.A. Frontini, M. Vazquez, M.B. Valcarce, Effective electrode preparation to prevent crevice in steel electrodes. https://doi.org/10.21203/rs.3.rs-3783347/v1, 2023.

[23] P. Ghods, O.B. Isgor, J.R. Brown, F. Bensebaa, D. Kingston, XPS depth profiling study on the passive oxide film of carbon steel in saturated calcium hydroxide solution and the effect of chloride on the film properties, Appl. Surf. Sci. 257 (2011) 4669–4677, https://doi.org/10.1016/j.apsusc.2010.12.120.

[24] G. Bhargava, I. Gouzman, C.M. Chun, T.A. Ramanarayanan, S.L. Bernasek, Characterization of the "native" surface thin film on pure polycrystalline iron: a high resolution XPS and TEM study, Appl. Surf. Sci. 253 (2007) 4322–4329, https://doi.org/10.1016/j.apsusc.2006.09.047.

[25] M. Descostes, F. Mercier, N. Thromat, C. Beaucaire, M. Gautier-Soyer, Use of XPS in the determination of chemical environment and oxidation state of iron and sulfur samples: constitution of a data basis in binding energies for Fe and S reference compounds and applications to the evidence of surface species of an oxidized pyrite in a carbonate medium, Appl. Surf. Sci. 165 (2000) 288–302, https://doi.org/10.1016/S0169-4332(00)00443-8.

[26] L.V. Duong, B.J. Wood, J.T. Kloprogge, XPS study of basic aluminum sulphate and basic aluminium nitrate, Mater. Lett. 59 (2005) 1932–1936, https://doi.org/10.1016/j.matlet.2005.02.029.

[27] S.C. Angulo, M.S. Guilge, V.A. Quarcioni, M.A. Cincotto, T.R.S. Nobre, H. Pöllmann, The role of calcium silicates and quicklime on the reactivity of rehydrated cements, Constr. Build. Mater. 340 (2022) 127625, https://doi.org/10.1016/j.conbuildmat.2022.127625.

[28] G. Jiang, E. Wightman, B.C. Donose, Z. Yuan, P.L. Bond, J. Keller, The role of iron in sulfide induced corrosion of sewer concrete, Water Res. 49 (2014) 166–174, https://doi.org/10.1016/j.watres.2013.11.007.

[29] L. Yohai del Cerro, W.H. Schreiner, M.B. Valcarce, M.V. Vazquez, Inhibiting steel corrosion in simulated concrete with low phosphate to chloride ratios. https://doi.org/10.1149/2.0511613jes, 2016.

[30] Z. Geng, Y. Liu, J. Shi, Electrochemical responses of carbon steel in ordinary Portland cement blended with calcium sulfoaluminate cement, Constr. Build. Mater. 400 (2023), https://doi.org/10.1016/j.conbuildmat.2023.132788.

[31] M.B. Valcarce, M. Vázquez, Carbon steel passivity examined in alkaline solutions: the effect of chloride and nitrite ions, Electrochim. Acta 53 (2008) 5007–5015, https://doi.org/10.1016/j.electacta.2008.01.091.

[32] M.B. Valcarce, C. López, M. Vázquez, The role of chloride, nitrite and carbonate ions on carbon steel passivity studied in simulating concrete pore solutions, J. Electrochem. Soc. 159 (2012) C244, https://doi.org/10.1149/2.006206jes.

[33] W. Xu, K. Daub, X. Zhang, J.J. Noel, D.W. Shoesmith, J.C. Wren, Oxide formation and conversion on carbon steel in mildly basic solutions, Electrochim. Acta 54 (2009) 5727–5738, https://doi.org/10.1016/j.electacta.2009.05.020.

[34] M.F. Montemor, A.M.P. Simões, M.G.S. Ferreira, Chloride-induced corrosion on reinforcing steel: from the fundamentals to the monitoring techniques, Cem. Concr. Compos. 25 (2003) 491–502, https://doi.org/10.1016/S0958-9465(02)00089-6.

[35] J.A. González, J.M. Miranda, N. Birbilis, S. Feliu, Electrochemical techniques for studying corrosion of reinforcing steel: limitations and advantages, Corrosion 61 (2005) 37–50, https://doi.org/10.5006/1.3278158.

[36] L. Yohai, M. Vázquez, M.B. Valcarce, Brass corrosion in tap water distribution systems inhibited by phosphate ions, Corros. Sci. 53 (2011) 1130–1136, https://doi.org/10.1016/j.corsci.2010.12.005.

[37] L. Yohai, M.B. Valcarce, M. Vázquez, Testing phosphate ions as corrosion inhibitors for construction steel in mortars, Electrochim. Acta 202 (2016) 316–324, https://doi.org/10.1016/j.electacta.2015.12.124.
[38] C. Andrade, M. Keddam, X.R. Nóvoa, M.C. Pérez, C.M. Rangel, H. Takenouti, Electrochemical behaviour of steel rebars in concrete: influence of environmental factors and cement chemistry, Electrochim. Acta 46 (2001) 3905–3912, https://doi.org/10.1016/S0013-4686(01)00678-8.
[39] S. Joiret, M. Keddam, X.R. Nóvoa, M.C. Pérez, C. Rangel, H. Takenouti, Use of EIS, ring-disk electrode, EQCM and Raman spectroscopy to study the film of oxides formed on iron in 1 M NaOH, Cem. Concr. Compos. 24 (2002) 7–15, https://doi.org/10.1016/S0958-9465(01)00022-1.